nature biotechnology

Article

https://doi.org/10.1038/s41587-026-03229-7

Engineered polyketide synthases enable a microbial chassis for recyclable plastics with tunable properties

Received: 21 February 2025

Accepted: 19 June 2026

Published online: 27 July 2026

Check for updates

Zilong Wang[1,2,3,16], Seokjung Cheong[1,2,3,16], Hai Wang[4,17], Jeremy Demarteau[4], Alexander R. Epstein[5,18], Baishakhi Bose[6], Weixi Hu[3,7,8], Matthias Schmidt[1,3,6], Leah Keiser[3,7], Mei Zhao[2,3,19], Beibei Ge[2,3,20], Alberto A. Nava[2,3], Ramu Kakumanu[3,6], Edward E. K. Baidoo[3,6], Yan Chen[3,6], Christopher J. Petzold[3,6], Yifan Guo[3,7,8], Nawa Raj Baral[3,6], Nemi Vora[3,6,21], Sarah L. Nordahl[9], Yuzhong Liu[1,2,3], Rithwik Ghanta[5,22], Pablo Cruz-Morales[3,6,10,11,23], Kevin Yin[3,6,12], Robert W. Haushalter[3,6], Kristin A. Persson[5,13], Corinne D. Scown[3,6,9,14], Brett A. Helms[3,4,13] & Jay D. Keasling[1,2,3,6,10,15]

Plastics derived from fossil feedstocks pose major recycling challenges, particularly crosslinked thermosets used in electronics, construction and composites. Polydiketoenamines (PDKs) are recyclable alternatives; however, monomers such as dimedone are petrochemical-derived and offer limited tunability. We computationally screened 144 β-keto-δ-lactones (BKDLs), identifying solvation free energy as the primary determinant of depolymerization temperature across a 20–60 °C range. We engineered hybrid type I polyketide synthases (PKSs) in *Escherichia coli* and *Streptomyces* hosts to biosynthesize BKDLs with diverse substituents and defined stereochemistry, reaching titers of 1.84 g L^{-1} in bioreactors. Polymerization of chemically synthesized BKDLs identical to PKS products confirmed tunable glass transition temperatures (53–98 °C) and temperature-gated depolymerization. Different BKDLs yielded PDKs with thermal, mechanical, solvent-resistance and optical properties governed by substituent and chirality. Technoeconomic and life-cycle analyses indicate that corn-stover-derived BKDLs can outperform petrochemical dimedone on cost and greenhouse gas emissions. This study demonstrates that engineered PKSs can produce monomers for recyclable plastics with programmable depolymerization behavior.

More than 400 million metric tons of plastics are produced annually, largely from fossil resources[1]. This amount is expected to double by 2050 (https://www.nationalgeographic.com/environment/article/plastic-pollution). As much as 20% of these plastics are thermosets, which incorporate additives, fillers and finishes that render the materials virtually unrecyclable[2]. While only 9% of plastic is recycled (https://www.oecd.org/environment/plastic-pollution-is-growing-relentlessly-as-waste-management-and-recycling-fall-short.htm), the leakiness of global recycling systems has resulted in staggering amounts of waste discharged into the environment. There, the breakdown of plastics releases toxic substances that pose great harm to health, biodiversity and the climate[3]. Not only is it an urgent priority to design future plastics that are more readily recycled to incentivize their collection for reuse, it is also important to produce them sustainably from nonfossil resources and to tailor their chemistry to control their properties, including their breakdown in recycling systems and the environment. To this

A full list of affiliations appears at the end of the paper. e-mail: keasling@berkeley.edu

end, polydiketoenamines (PDKs)[4] have recently emerged as circular thermoplastics, crosslinked thermosets, elastomers, adhesives and composites[4–6], where greenhouse gas (GHG) emissions that result from recycling PDKs are lower than those tied to primary production of commodity polymer resins from fossil feedstocks[7]. However, current PDK monomers such as dimedone are derived from petrochemicals and cost approximately 10 US$ per kg, which is a counterpoint to the sustainability case for these emerging recycle-by-design materials. Moreover, the limited structural diversity of available monomers restricts tuning of the glass transition temperature (T_g), solvent resistance and mechanical properties and there is no systematic way to program depolymerization temperature to enable staged recycling of mixed-plastic streams. A detailed comparison of previously reported PDK systems is provided in Supplementary Table 1. Previously, we showed that PDKs can be produced from triacetic acid lactone (TAL)[8]; however, TAL-based PDKs do not allow tailoring of polymer properties through substituent choice or stereochemistry.

The ability to tune PDK properties is critical for practical applications. For example, electronics demand high T_g for hardness and dimensional stability, while packaging requires low T_g for flexibility. Solvent resistance is also important, which typically requires tunability in hydrophobicity. The γ-substituent and δ-substituent on β-keto-δ-lactone (BKDL) monomers open the door to controlling hydrophobicity and, therefore, solvent resistance; these measures also affect depolymerization temperature as acidolysis involves the ingress of a highly polar reactive medium within the material during deconstruction. With regard to tunability in T_g and optical appearance, enantiomerically pure chiral BKDLs open the door to controlling packing in the condensed phase in a manner not achievable with a racemic mixture and may enable more amorphous, optically clear PDKs. Taken together, access to chiral BKDLs and BKDL-PDKs therefrom represents a rare yet compelling strategy for accessing thermal properties, chemical resistance, optical clarity and temperature-gated staged recycling (spanning 0–60 °C) to access reusable biobased monomers. Moreover, a single microbial chassis capable of producing different BKDLs to supply monomers for diverse markets while maintaining full recyclability is, therefore, highly desirable; this is the platform value of a biosynthetic approach.

Here, we show that, by engineering type I polyketide synthases (PKSs), we gain access to a broad range of BKDLs with different substituents and defined stereochemistries at the γ-position and δ-position and, in stride, polymer properties (Fig. 1). In this study, we (1) computationally screen 144 BKDLs and identify solvation free energy ($\Delta G_{solvation}$) as the primary determinant of depolymerization temperature; (2) engineer hybrid type I PKSs to biosynthesize BKDLs with diverse substituents and defined stereochemistry, reaching titers of 1.84 g L^{-1} in bioreactors; (3) polymerize chemically synthesized BKDLs—identical to PKS products—into PDKs and validate tunable T_g (53–98 °C) and temperature-gated depolymerization (0–60 °C); (4) demonstrate that different BKDLs yield PDKs with distinct thermal, mechanical and solvent-resistance properties enabling staged recycling of mixed-plastic streams; and (5) conduct technoeconomic analyses (TEAs) and life-cycle assessments (LCAs) showing that BKDL production from corn stover achieves lower costs and GHG emissions than petrochemical dimedone. The overall workflow integrating computational prediction, biosynthetic design and material testing is summarized in Supplementary Fig. 1, which illustrates the progressive narrowing from a theoretical BKDL design space to experimentally validated BKDL-PDKs. We tested the predictions by synthesizing a series of chiral and achiral PDKs from chemically synthesized BKDLs—three of them structurally identical to the BKDLs produced by our engineered PKSs—and used the results to identify the simulation parameters most informative for PDK recycling outcomes. All PDKs characterized in this study were polymerized from these chemically produced BKDL monomers; the biosynthetic platform demonstrated here is designed to replace these chemical routes at commercial scale. Compared to TAL-based BKDL-PDKs synthesized from TAL and sebacic acid—for which the T_g is 132 °C and the depolymerization temperature is 25 °C—our expanded series of chiral BKDL-PDKs derived from BKDLs exhibited broad tunability in thermal properties (53–98 °C) and deconstruction temperatures (0–60 °C). We offer insights into future BKDL designs accessible through the recombination of PKSs, enabling the use of our microbial chassis to diversify BKDLs to meet different market demands for PDKs—something that would be nearly impossible to do at scale using synthetic chemistry. In our systems analysis, we further present scenarios for advancing BKDL production from discovery to commercial-scale manufacturing, which comes at a critical juncture, given the growing interest in biomanufacturing products, particularly sustainable plastics from abundant renewable feedstocks, such as agricultural and forest waste.

The counterpoint to this is the chemical synthesis of chiral BKDLs, which requires expensive reagents, pyrophoric conditions and multistep stereoselective sequences (for example, Evans aldol reactions with chiral auxiliaries), rendering these routes impractical at commodity scale. Engineered type I PKSs offer a fundamentally different approach; their modular architecture sets both substitution pattern and stereochemistry in a single enzymatic step through module and domain recombination, making diverse chiral BKDLs accessible for the first time through fermentation. Moreover, TEAs and LCAs show that bio-BKDLs produced from corn stover are already projected to be cheaper and lower in GHG emissions than petrochemical dimedone, even at currently demonstrated yields. This approach advances beyond prior computational work on PDK design by introducing $\Delta G_{solvation}$ as a new predictive variable for depolymerization behavior, screening 144 structurally diverse BKDLs and coupling computational predictions to biosynthetic production, TEAs and LCAs.

Results

Biosynthesis of BKDLs using engineered PKSs

We constructed and tested BKDL synthases using parts from type I modular PKSs, multidomain enzymes that synthesize polyketides from acyl-CoAs in an assembly-line manner. BKDLs can be synthesized using relatively small PKSs containing a loading module, two extension modules and a thioesterase (TE) that cyclizes the lactone ring during hydrolysis of the product from the synthase (Fig. 2a). While it is essential for the α-carbon of the BKDL to be unsubstituted and β-carbon to be a ketone, the γ-carbon and δ-carbon can be functionalized with various pendant groups. Additionally, the stereochemistry of those two positions can be specified by the PKS[9,10]. These features can be used to tailor polymer properties, although this remains unexplored.

We used a PKS design software, ClusterCAD[11,12], and genome mining to predict candidate PKS domains, modules and TEs needed to produce a diverse set of BKDLs **2**–**11** (Fig. 2b). PKS modules and domains were chosen to perform the chemistry needed to produce BKDLs from acyl-CoAs that are naturally available or whose biosynthesis could be engineered into bacteria. The functionality on the δ-carbon is specified by the PKS loading module; the functionality at the γ-position is specified by the first extension module and the ketoreductase (KR) in that module specifies the stereochemistry at the γ-position and δ-position. Because some acyltransferases (ATs) are promiscuous for the malonyl-CoA analogs that they accept, it is possible to expand the range of BKDLs (different substitutions on the δ-carbon) by producing various malonyl-CoA analogs in the cell expressing the PKS with the promiscuous AT, a property that we exploited to produce several BKDLs in vitro (Supplementary Fig. 2b,c and 3). As BKDLs must have a β-keto group and a methylene at the α position, extension module 2 must be nonreducing (no functional KR domain) and use malonyl-CoA as the extension substrate[13]. There are few natural PKSs that have a module with the features required of that extension module; thus, we used three hybrid extension module 2s with different degrees of alterations

https://doi.org/10.1038/s41587-026-03229-7

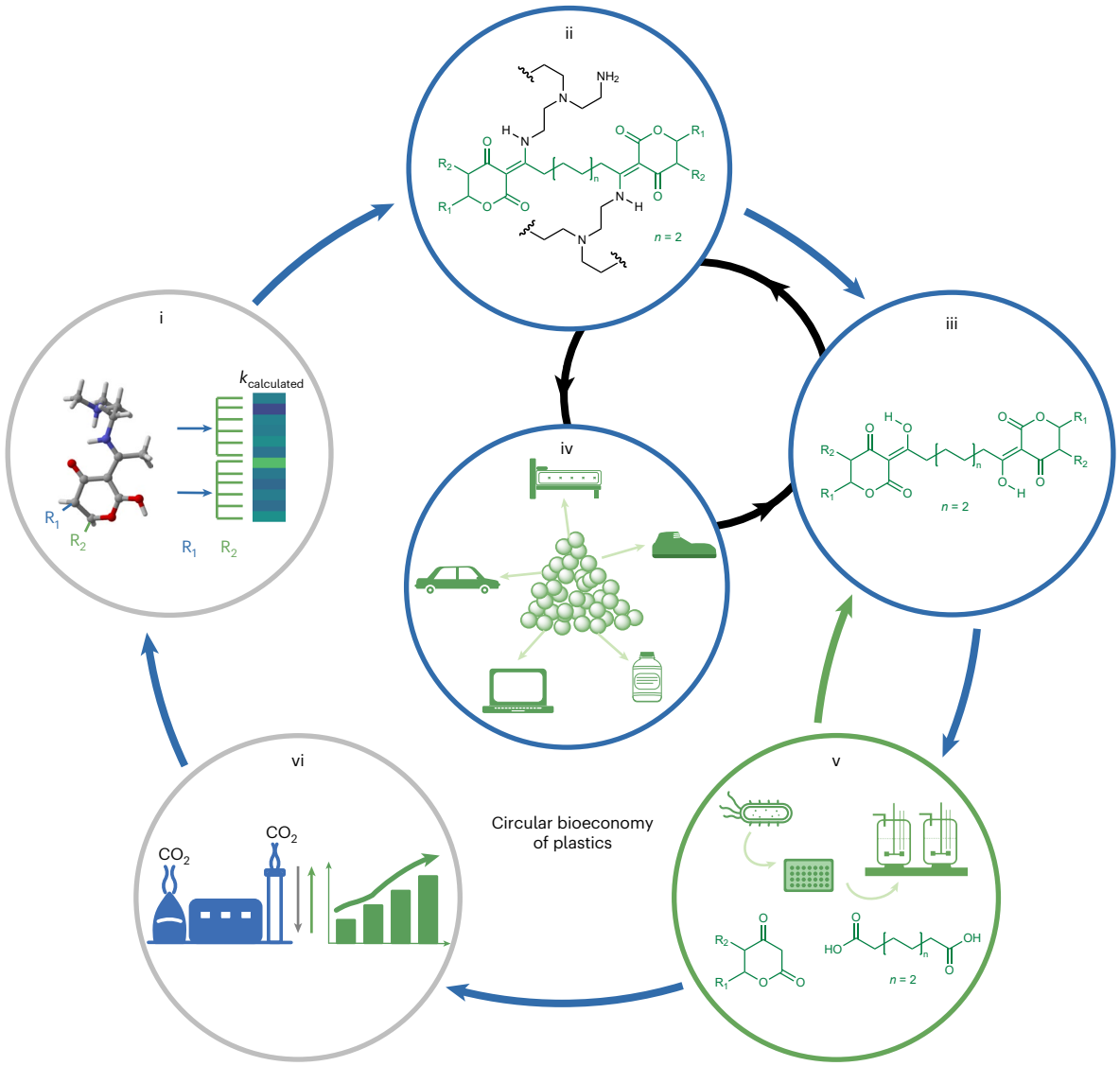

Fig. 1 | Workflow (blue arrows) to identify useful circular BKDL-PDK plastics (black arrows) produced from biorenewable feedstocks (green circle and arrow). Computation screens of diketoenamine bond hydrolysis and $\Delta G_{solvation}$ (**i**) are predictors of BKDL-PDK recycling behaviors and inform monomer designs (**ii**,**iii**). These monomers can be synthesized from diverse BKDLs and diacids, produced biologically using hybrid PKSs expressed in engineered bacteria from inexpensive sugars and other biorenewable feedstocks (**v**). Triketone monomers (**iii**) synthesized from these precursors are then polymerized with amine monomers, for example, with *tris*(2-aminoethyl)amine, to yield rigid BKDL-PDK plastics (**iv**). BKDL-PDKs are chemically recycled in strong acid (**iv** → **iii**), returning the original triketone and amine monomers, permitting their reuse in circular manufacturing. TEAs and LCAs (**vi**) provide insights into MSP and GHG emissions of the virgin and recycled PDKs, levelized over the number of remanufacturing cycles achievable as a function of the observed material efficiency.

to investigate BKDL biosynthesis (Supplementary Fig. 4): extension module 2 of the rifamycin PKS (rifM2)[14] can be used in its native form; extension module 1 of the mycolactone synthase B1 (mlsB1)[15] naturally extends with malonyl-CoA but its KR must be inactivated; and extension module 6 of the erythromycin PKS (debsM6)[16] natively extends with methylmalonyl-CoA, whereby its AT must be exchanged with one that favors malonyl-CoA (for example, epothilone PKS extension module 4 AT, epoAT4)[17] and its KR must be mutated to eliminate its activity. In vitro biosynthesis of BKDL **7** with purified enzymes was demonstrated before implementation of the in vivo BKDL production (Supplementary Figs. 2c and 4). BKDLs **9**–**11** (Supplementary Fig. 3) were produced in vitro by supplementing lysates of *Escherichia coli* expressing the PKSs (strains sZWe01, sZWe03 and sZWe04 for BKDLs **9** and **10**; sZWe02, sZWe03 and sZWe04 for BKDL **11**) with acetyl-CoA, malonyl-CoA and methylmalonyl-CoA (BKDL **9**), acetyl-CoA and malonyl-CoA (BKDL **10**) and propionyl-CoA, malonyl-CoA and allylmalonyl-CoA (BKDL **11**).

In *E. coli* K207-3 (ref. 18), PKSs with debsM1 as first extension module and rifM2 as the second extension module (strain sSC05_1; Supplementary Table 2) produced 200 μg L^{-1} BKDL **4** (Fig. 2c and Supplementary Figs. 5b and 6b), while PKSs with lipM1 as first extension module and debsM6 (epoAT4, KRnull) as the second extension module (strains sSC22_1 and sSC22_2) produced 100–220 μg L^{-1} BKDL **5**, depending on the copy number of the two modules (Supplementary Fig. 5c). Given the low titers of BKDLs **4** and **5** produced by *E. coli* (Supplementary Fig. 5b,c), we tested five *Streptomyces* spp. (*S. albus*, *S. lividans*, *S. coelicolor*, *S. venezuelae* and *S. noursei*) for the production of BKDLs. The genes encoding lipLM-lipM1 and mlsB1*-debsTE, which showed the best performance in the in vitro assay, were integrated into their genomes to produce BKDL **8**. In 7-day cultures, *S. albus* produced the highest titer of BKDL **8**, ~2 mg L^{-1}, while other species produced more early termination product, 3-hydroxy-2, 4-dimethyl-pentanoic acid, >300 mg L^{-1}, but much less BKDL **8**, <0.1 mg L^{-1} (Supplementary Fig. 5e). The low production was likely

https://doi.org/10.1038/s41587-026-03229-7

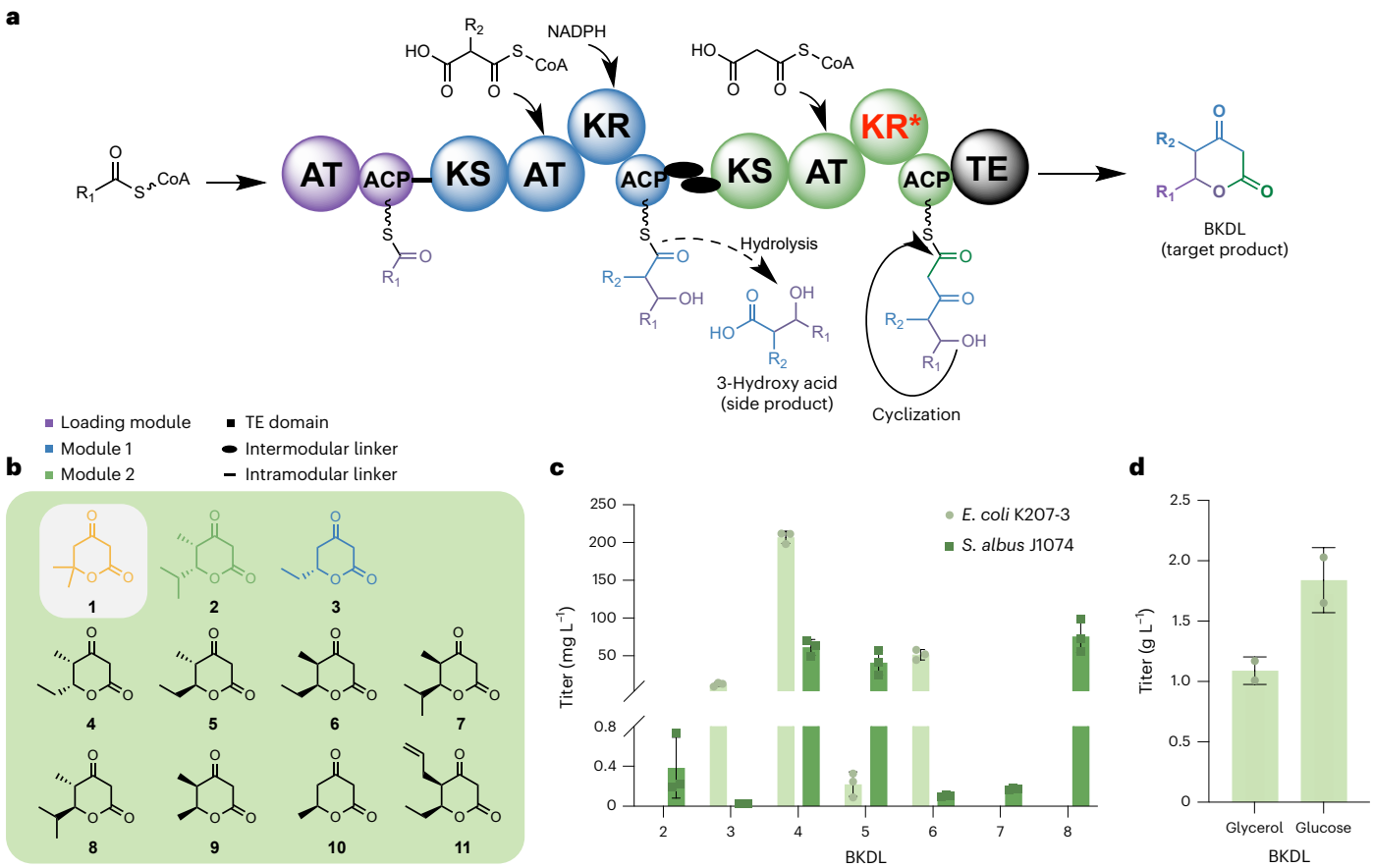

Fig. 2 | Engineered PKSs produce BKDLs. a, Biosynthesis pathway of BKDLs with recombined PKSs. All substrates are CoA derivatives, including the starter unit and extension units. Module 2 must use malonyl-CoA (for the α-carbon to be a methylene) and be nonreducing (for the β-carbon to be a ketone). The extended polyketide can potentially be hydrolyzed off module 1, resulting in the side product of 3-hydroxy acids. **b**, All BKDLs produced in this study, except chemically synthesized BKDL **1**. **c**, Titers of BKDL production from *E. coli* K207-3 (light-green bars) and *S. albus* J1074 (dark-green bars). Detailed productions are presented in Supplementary Figs. 5b–f, 10a–g and 12b. The products and corresponding *E. coli* and *S. albus* strains (Supplementary Table 2) that produced the above titers are as follows: **2**, N.A., sZW37_1; **3**, sSC30_1, sZW35_1; **4**, sSC26_1, sZW26_1; **5**, sSC22_2, sZW23_1; **6**, sSC27_2, sZW37_1; **7**, N.A., sZW39_1; **8**, N.A., sZW44_1 (N.A. indicates that no product was detected for any strain). Data are presented as the mean values ± s.d. from three biologically independent experiments. **d**, Titer of BKDL **4** produced by *E. coli* strain sSC26_2 in 1-L batch reactor cultivations using LB-EZ-Rich medium containing either glucose or glycerol as carbon sources. Data are presented as the mean values ± s.d. from two biologically independent 1-L bioreactor fermentation experiments. R*, inactive KR.

because of the low expression of the second extension module (Supplementary Fig. 7), considering that the intracellular level of malonyl-CoA is one of the most abundant CoA thioesters in *S. albus* J1074 (ref. 19). Interestingly, nearly 90% of the BKDL and 3-hydroxy acids were secreted from the cells (Supplementary Fig. 7a). Feeding cells [^{13}C]L-valine enabled us to further confirm the identity of the products (Supplementary Figs. 8b and 9). Consistent with the in vitro results, the best extension module 2 in *S. albus* was mlsB1*-debsTE (Fig. 2c and Supplementary Fig. 10f). The titer reached 27.5 mg L^{-1} on the 11th day (Supplementary Fig. 10a).

With the detection of over 100-fold more 3-hydroxy acid intermediates than BKDL, we suspected that the transfer of the 3-hydroxy diketide from the first extension module to the second might be limited. Therefore, we fused the first and second extension modules, creating a single, large hybrid PKS. Ten recombined PKSs were designed (PKSs 31–40, Supplementary Table 3) to produce BKDLs with substitutions of ethyl (BKDLs **4**–**6**) and isopropyl (BKDLs **2**, **7** and **8**) groups at the δ position and with methylene or a methyl group at the γ-position. When integrated into *S. albus*, the engineered PKSs produced the desired BKDLs. While the fusion strategy ensured that extension modules 1 and 2 were expressed at the same level, it resulted in very low titers of BKDL (<0.5 mg L^{-1}) (Supplementary Fig. 10b–g). We hypothesized that the interaction between the acyl carrier protein (ACP) in the first extension module and the ketosynthase (KS) in the second extension module may be compromised by the linker between the two domains and/or by a mismatched interaction between the ACP and KS (Supplementary Fig. 11). Hence, we exchanged the mlsB1 KS in extension module 2 with the KS from the lipomycin module 2 (M2_lipKS2 swap) and deleted the KR from mlsB1 (M2_KR2 deleted). The resulting constructs (strains sZW46_1 and sZW44_1) produced 16.5 and 78.2 mg L^{-1} BKDL **8**, respectively, with the KR deletion having a more notable impact on BKDL production than the KS exchange (Supplementary Fig. 12).

Additionally, we expressed parts of the pikromycin biosynthetic gene cluster (Pik127 or Pik167), which have been reported to produce triketide lactones similar to BKDLs but containing an α-methyl[20]. We replaced the methylmalonyl-CoA-specific AT of pikromycin module 6 with malonyl-CoA-specific borrelidin module 1 AT (borAT1) or with the pikromycin module 2 AT (pikAT2). The resulting *E. coli* K207-3 strains (strains sSC27_2, sSC26_1 and sSC30_1) expressing these constructs produced ~50 mg L^{-1} BKDL **6**, ~200 mg L^{-1} BKDL **4** and ~12 mg L^{-1} BKDL **3**, respectively (Supplementary Fig. 5d). We then integrated these constructs into *S. albus* and achieved titers of 61.4 mg L^{-1} BKDL **4** (Fig. 2c), still with the second extension module poorly expressed. The overall increase in BKDL titers in *E. coli* was attributed to the much higher soluble expression of pikromycin PKSs; increasing the copy

https://doi.org/10.1038/s41587-026-03229-7

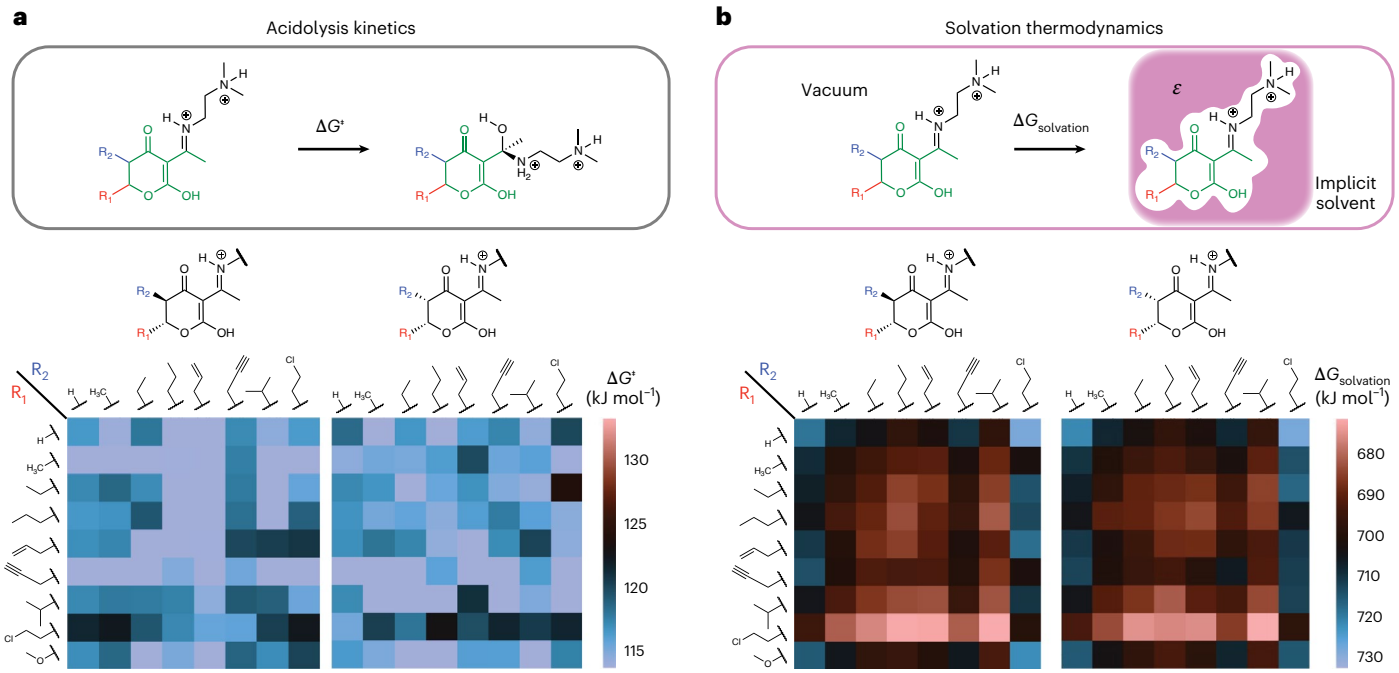

Fig. 3 | Assessing effects of BKDL functionalization and stereochemistry on kinetics and thermodynamics of BKDL-PDK hydrolysis. a,**b**, Heat maps for calculated $\Delta G^{\ddagger}$ (**a**) and $\Delta G_{solvation}$ (**b**) for small molecules representing ionizable and hydrolyzable bonds in circular BKDL-based PDKs. $\Delta G^{\ddagger}$ evidenced no notable variation with substitution, whereas $\Delta G_{solvation}$ trended with substituent size.

number of the plasmid harboring module 2 so that the level of module 2 protein was comparable to that of module 1 reduced the amount of side product 3-hydroxy acid (Supplementary Fig. 7b). Further integration of genes encoding malonyl-CoA synthetase and transporter, MatBC, into the K207-3 genome to increase malonyl-CoA supply[21] and scaling of the cultivation process to 1-L bioreactors successfully increased the titers of BKDL **4** to 1.09 g L^{-1} with glycerol (consumption of 12.05 g L^{-1} glycerol, 20.0 mM sodium propionate and 5.5 mM sodium malonate supplemented) and 1.84 g L^{-1} with glucose (consumption of 15.86 g L^{-1} glucose, 9 mM sodium propionate and 0.1 mM sodium malonate supplemented) as the primary carbon source in just 24 h (Fig. 2d and Supplementary Fig. 13), with 9.4% and 21.2% of the theoretical maximum yield, respectively (Supplementary Methods). Taken together, we demonstrated production of ten different BKDLs, both in vitro (Supplementary Fig. 3) and in vivo (Fig. 2c), and one of these BKDLs was scaled in bioreactors to nearly 2 g L^{-1}. While these titers are still low relative to what would be needed for commercial production, they are a good starting point for further optimization.

Design, synthesis and testing of chiral BKDL-PDKs made from BKDLs

Having identified type I PKSs that produce BKDLs, we sought to develop a computational platform that could inform how the different substituents and their respective stereochemistries might impact the properties of PDKs derived therefrom. This would allow specific targets to be prioritized for recycling circularity. For example, there are two plausible mechanisms by which substituents might affect recycling circularity: (1) remote substituent effects can dictate the structure and free energy of the acidolysis transition state, relative to starting materials and products and (2) changes in hydrophobicity might affect the $\Delta G_{solvation}$ of the diketoenamine during acidolysis, limiting water uptake and reactive surface area.

We selected 144 functionally and stereochemically diverse BKDLs with functional groups that are found in natural polyketides: eight substituents at the δ-position and nine substituents at the γ-position in both *cis* and *trans* configurations. To provide context for the first mechanism, we carried out density functional theory simulations of the reaction coordinates for acidolysis of small-molecule diketoenamines, calculating the standard free energy of activation ($\Delta G^{\ddagger}$) for the addition of water to the iminium intermediate along the reaction coordinate[5,22] (Supplementary Tables 4 and 5). We used multipath transition state theory[23,24] to ensure the highest level of agreement between theory and experiment. To provide context for the second mechanism, we calculated $\Delta G^{\ddagger}$ and $\Delta G_{solvation}$ of ionized diketoenamine bonds, which is affected by the hydrophobicity imparted by the substituents (Supplementary Tables 6 and 7). Through these calculations, we found that the γ-substituent and δ-substituent, regardless of stereochemistry, did not substantially alter $\Delta G^{\ddagger}$ because they produce relatively small changes to molecular conformation near the reaction center (Fig. 3a). However, $\Delta G_{solvation}$ has a more important role than previously recognized in BKDL-PDK recycling behaviors. Notably, even small differences in ΔG translate to large differences in reaction rates through Eyring scaling (rate ∝ $\exp(-\Delta G^{\ddagger}/RT)$) and these thermodynamic effects are further amplified in the solid polymer by morphology-dependent and transport-dependent access of water and acid to the diketoenamine bonds (Fig. 3b).

To test these hypotheses, we chemically synthesized achiral BKDL **1** from methyl acetoacetate and acetone, as well as four chiral BKDLs bearing unique substituents at the δ-position and γ-position (R_1 and R_2, respectively) (Fig. 4a). BKDLs **2**, **3** and **3′** were chosen because they can be biosynthesized using engineered PKSs and have differences in both steric effects on the transition state and emergent hydrophobicity (Fig. 3). We prepared chiral BKDL **2** bearing an isopropyl and a methyl substituent at the δ-position and γ-position, respectively, using a sequence that included an enantioselective Evans aldol reaction, acylation of the α-alkyl-β-hydroxy oxazolidin-2-one and Claisen condensation from the kinetic enolate, which liberates the chiral auxiliary. For chiral BKDL **3** bearing an ethyl substituent at the δ position, we conducted a catalytic asymmetric vinylogous Mukaiyama aldol reaction followed by base-promoted ring closure to the desired chiral lactone. As a control, we synthesized BKDL **3′** (racemic mixture) bearing an ethyl substituent at the δ-position from methyl acetoacetate and

https://doi.org/10.1038/s41587-026-03229-7

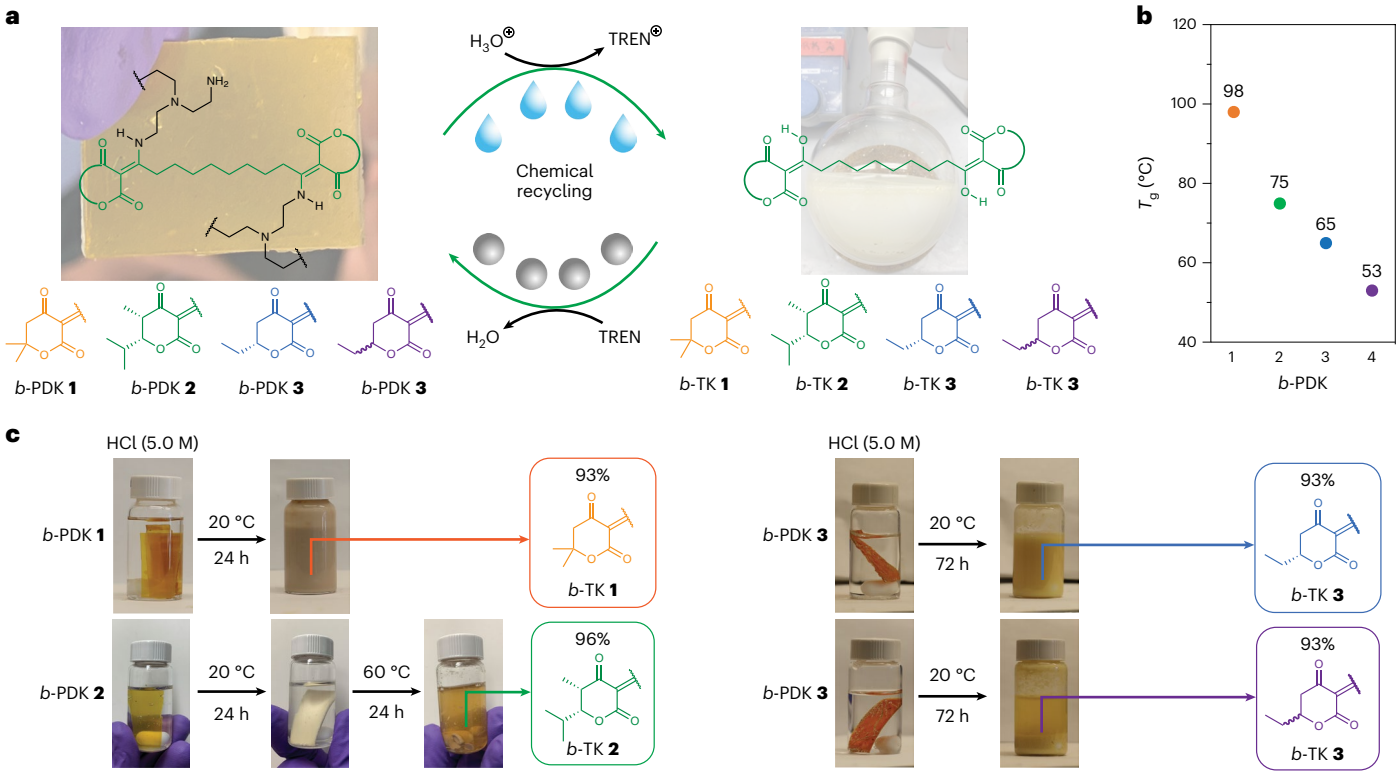

Fig. 4 | Experimental validation of circular BKDL-based BKDL-PDKs. **a**, Photograph of a BKDL-PDK film held between thumb and forefinger, demonstrating the material's flexibility and optical clarity. Chemical synthesis of *b*-PDK **1**–**3** and **3′**. **b**, T_g of *b*-PDK **1**–**3** and **3′** assessed by differential scanning calorimetry. **c**, Acid-catalyzed depolymerization of *b*-PDK **1**–**3** and **3′** and recovery of their corresponding monomers at specific temperature thresholds.

propionaldehyde. These synthetic sequences serve as reference points for how challenging it would be to manufacture BKDLs as a commodity chemical at scale, which motivates a biosynthetic route that obviates expensive reagents and pyrophorics.

Condensation of these BKDLs (BKDLs **1**–**3**/**3′**; Fig. 4) with sebacic acid provided the corresponding triketones: *b*-TK **1** (achiral control), *b*-TK **2** (isopropyl chiral and hydrophobic), *b*-TK **3** (ethyl chiral) and *b*-TK **3′** (ethyl racemic mixture). These triketones were then polymerized with *tris*-(2-aminoethyl)amine to yield *b*-PDK **1**–**3** and **3′** (refs. 4–6) (Fig. 4a). The materials exhibited different T_g; while *b*-PDK **1** showed a T_g of 98 °C, *b*-PDK **2** showed a T_g of 75 °C and *b*-PDK **3** and **3′** exhibited T_g of 65 and 53 °C, respectively (Fig. 4b). The chemical recycling of *b*-PDK **1** in 5.0 M HCl to triketone *b*-TK **1** (93% yield) was complete after 24 h at room temperature (Fig. 4c)[4–6]. Notably, in contrast, hydrolysis of *b*-PDK **2** under the same conditions was arrested; instead, the sample retained its integrity but whitened over time as the sample swelled slightly and began to scatter visible light. To promote hydrolysis, we raised the depolymerization temperature to 60 °C, after which complete deconstruction of *b*-PDK **2** to *b*-TK **2** (96% yield) was observed after 24 h (Fig. 4c). *b*-PDK **3** and **3′** displayed slightly slower deconstruction rates than *b*-PDK **1**, as the complete deconstruction of the networks into their corresponding *b*-TK **3** and **3′** components required 72 h (both with 93% yield of recovered monomer). While we observed differences in structure and thermal properties, we did not find that chirality influenced the yield (Fig. 4a) or purity (^{1}H nuclear magnetic resonance analysis in Supplementary Fig. 14) of recovered *b*-TK monomers after PDK deconstruction in strong acid; all were comparably high.

As our goal was to develop a design model to choose BKDLs on the basis of desired polymer properties, we compared the experimental and computational results. *b*-PDKs **1**, **2** and **3** had negligible differences in computed $\Delta G^{\ddagger}$ relative to *b*-PDK **1**, 0.36 and 3.18 kJ mol^{-1}, respectively, which did not account for the observed differences in PDK deconstruction rate (Supplementary Table 8). Considering the notable differences in $\Delta G_{solvation}$ observed with the γ-substituent and δ-substituent across the screening study and the consistency in ordering *b*-PDKs **1**, **2** and **3** between experiment and $\Delta G_{solvation}$ (Supplementary Table 9), we conclude that the differentiated rates of *b*-PDK acidolysis (Fig. 4c) are tied to the energetic costs of ionizing and solvating diketoenamine residues, rather than remote substituent effects tied to γ-methyl and δ-isopropyl substituents in *b*-PDK **2**. Moreover, expanding the opportunities of BKDL functionalization opens the door to mixed-plastic and composite recycling; because different BKDL-PDKs depolymerize at different temperatures, mixed streams containing multiple BKDL-PDK types can be recycled by sequential temperature steps, recovering each monomer cleanly at its specific threshold. The increase in hydrophobicity can also be exploited for chemical and solvent resistance (Supplementary Fig. 15).

Cost of BKDL production and paths for improvement

Commercializing BKDL-PDKs requires that they compete with incumbent plastics or thermosets on the basis of environmental impacts and cost, quantified here as minimum selling price (MSP). To develop a preliminary understanding of the cost and identify opportunities for improvement, we conducted a TEA. Integrating this analysis as part of the study allows us to gauge its scalability and determine how improvements in the titer, rate, yield and other process conditions will impact the potential for commercializing BKDL-PDKs (Fig. 5a). To this end, we analyzed three different scenarios: production of BKDL at 21% (based on experimental data), 50% (intermediate level of optimization) and 90% (fully optimized) of the maximum theoretical yield at commercial scale (Fig. 5b). Commercial scale was defined on the basis of a corn stover input of 2,000 bone-dry metric tons per day, meaning that the intermediate scenario produces around 65,670 metric tons

https://doi.org/10.1038/s41587-026-03229-7

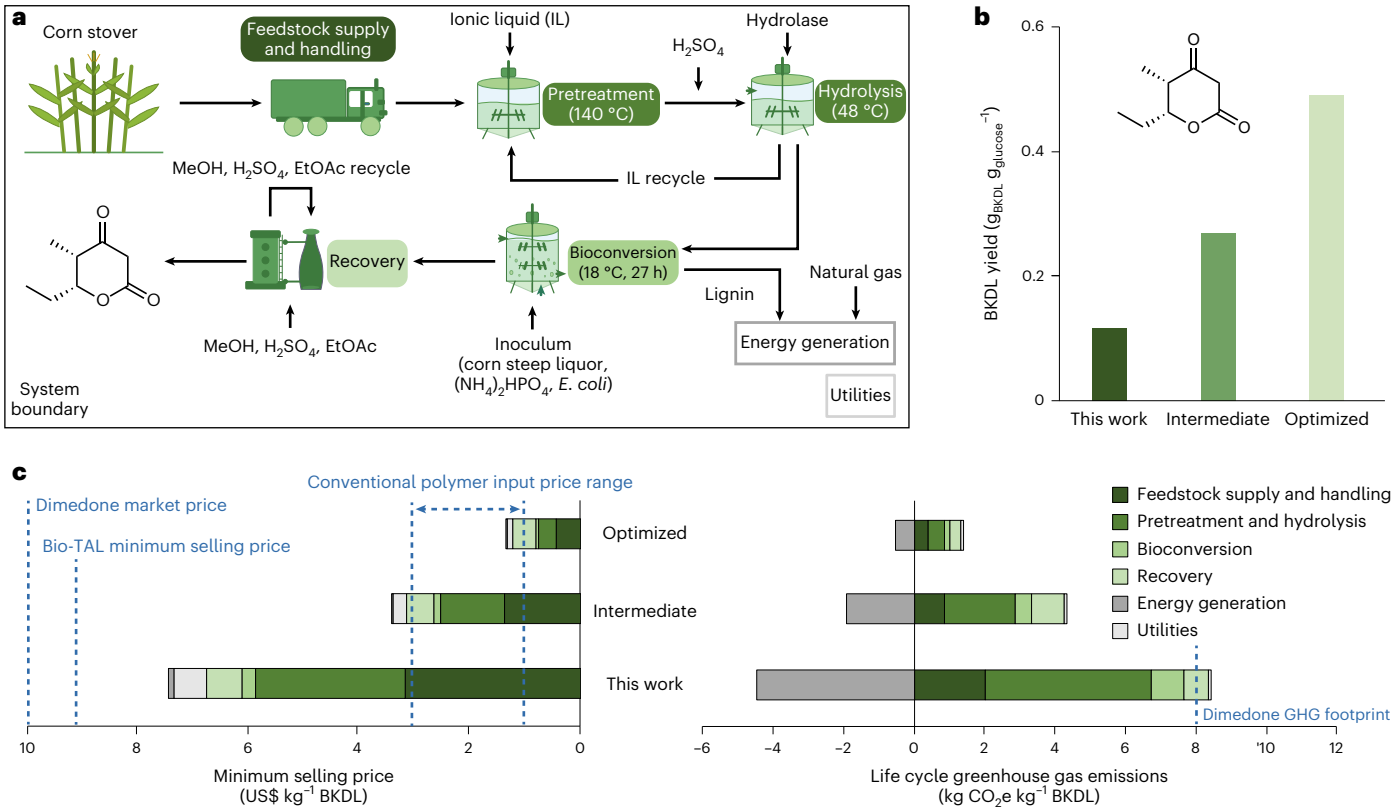

Fig. 5 | Systems analysis of BKDL bioproduction at commercial scale. a, Schematic systems boundary for BKDL bioproduction. **b**, Annual BKDL bioproduction and yield under the different scenarios, adjusting for factors such as the product yield and projected efficiencies gained at industrial scale. **c**, MSP and life-cycle GHG emissions for this work, as well as intermediate and fully optimized BKDL bioproduction at commercial scale. The dashed lines in **c** show the MSP and life-cycle GHG emissions per kg of dimedone for comparison, as well as the lowest-achieved MSP for TAL in Demarteau et al.[8] and an approximated market price range of 1–3 US$ per kg for raw material inputs, including polyols, propylene, isocyanates and ethylene, for commodity polymers (which are not functionally equivalent but useful frames of reference).

of BKDL per year, enough to meet the needs of multiple BKDL-PDK production facilities.

To place BKDL-PDKs in a broader economic context, we compared their production costs to multiple benchmarks, including dimedone and TAL (Fig. 5c). In BKDL-PDK production, BKDLs serve as a replacement for dimedone, a petrochemical priced at 10 US$ per kg. In our analysis, we found that BKDL production in all three different scenarios analyzed in this study achieves a lower MSP relative to the market price for dimedone (Fig. 5c). Our results suggest that commercial-scale BKDL production from corn stover can reduce the cost of PDK in the near term, even at the currently demonstrated yield (21% of theoretical maximum), provided a bioconversion residence time at or below 27 h. The MSP for BKDL based on the currently demonstrated yield is also approximately 1 US$ per kg lower than what was previously reported for TAL using a similar process configuration[8] and more than 3 US$ per kg less than the best-reported TAL performance before that study[25]. We include an approximated range of 1–3 US$ per kg in Fig. 5c as a useful frame of reference, indicating that a fully optimized BKDL production route can even compete in these mature petrochemical markets.

Life-cycle GHG emissions

With respect to GHG emissions, the three scenarios analyzed in this study result in lower cradle-to-gate GHG emissions compared to dimedone, reaching approximately 4 kg CO_2e per kg of BKDL considering experimental yield and 2.3 and 1.0 kg CO_2e per kg of BKDL in the intermediate (reaching 50% of theoretical maximum BKDL yield) and optimized (90% theoretical yield with other minor process optimizations) scenarios, respectively (Fig. 5c). The GHG results for BKDL reported here are considerably lower than previously reported GHG emissions for TAL production based on a similar configuration (which totaled 14 kg CO_2e per kg)[8], already a substantial reduction relative to the previously reported performance corresponding to 22 kg CO_2e per kg)[8,25]. More detailed waterfall plots for cost and GHG emissions can be found in Supplementary Fig. 16. Across all scenarios, lowering on-site energy use and/or purchasing 100% renewable electricity is key to reducing the GHG footprint of BKDL bioproduction. Minimizing bioconversion residence time and maximizing product yield are both essential to this energy demand and emissions reduction goal.

Opportunities for cost and emissions reductions

While BKDL production is currently growth coupled, exploring future decoupled growth and production phases could enable more cost-effective two-stage bioconversion with simplified media and lower aeration rate in the production phase. Maximizing product yield can also ensure that the substantial contributions from feedstock supply and handling, while pretreatment and hydrolysis remain low enough to ensure the GHG footprint of BKDL is below that of dimedone.

Residence time, which relates to the production rate, is also important for both the cost and GHG emissions; the electricity required to aerate and agitate the bioreactor while it is operating is a substantial contributor to emissions and the bioreactor capital costs are also dependent on residence time. Use of alternate hosts such as industry-favored *Corynebacterium* may reduce the time in the bioconversion reactor, which in turn will reduce the MSP. Improving the rate

and, thus, reducing bioconversion time can also lower the amount of on-site energy required, which further reduces the MSP.

Product recovery is a critical area for improvement. Column chromatography is currently used for BKDL recovery at laboratory scale and we have conservatively included this method in our model because of its demonstrated success in achieving sufficient purity. However, this approach is impractical for commercial production. Crystallization or precipitation of BKDL monomers represents the commercially relevant purification strategy, as the relatively low aqueous solubility of BKDLs with hydrophobic substituents is expected to facilitate direct recovery from fermentation broth. Transitioning from chromatography to crystallization-based recovery would substantially reduce both capital and operating costs (5.4% and 12% decreases in fixed capital investment and total operating costs, respectively; more details in Supplementary Fig. 16).

Additional improvements across the production system, including improved corn stover supply chain, improved sugar yields, higher ionic liquid and product recovery rates and enhanced titer, rate and yield are needed to reach the ambitious 'optimized' costs. The MSP of 1.34 US$ per kg of BKDL in the optimized scenario represents a practical minimum, beyond which further improvements would be nearly impossible, and can be useful in screening for commercially viable BKDL applications. Although the fully optimized scenario may not be achieved in the near term, the insights from this analysis provide useful near-term, mid-term and long-term achievable goals for BKDL bioproduction and process development.

Pathways to commercialization

Although this article discusses BKDLs in relation to a range of products, they are not functionally interchangeable for any of the comparators shown in Fig. 5c. BKDLs offer more tunability in terms of BKDL-PDK properties and hydrolysis conditions; thus, they are functionally superior to dimedone. This tunability, influenced by γ-substituent and δ-substituent variation, is further demonstrated by the broader depolymerization temperature range (20–60 °C) observed in BKDL-PDKs, along with T_g ranging 53–98 °C (Fig. 4a,b). While virgin commodity plastics (high-density polyethylene (HDPE), poly(ethylene terephthalate) (PET) and polypropylene (PP)) are typically priced at 1–2 US$ per kg, the key advantage of PDKs is their ease of recycling to virgin-quality monomers; previously published results show that the price of circular PDK (1.5 US$ per kg) is competitive with other commercial plastics such as HDPE (2.3 US$ per kg), polyurethane (PU) (4 US$ per kg) and PET (1.2 US$ per kg). TAL-based bio-PDKs have a reported optimized MSP of ~2 US$ per kg with GHG emissions of ~14 kg CO_2e per kg; BKDL-based PDKs substantially improve on both metrics. The key to commercialization (and a major challenge to overcome) is finding market applications that guarantee high rates of recovery for PDKs, as their low cost and ease of recycling are core elements to their competitiveness and environmental promise. Durable goods where centralized facilities reclaim large-scale components for recycling, such as automotive parts, could be one such application.

Discussion

Recycling commodity thermoplastics, particularly PET, HDPE and PP, is increasingly practiced, while crosslinked materials remain an outstanding challenge. PDK materials offer inroads to crosslinked polymer deconstruction in a manner tolerant to a wide range of additives and fillers, returning the original monomers in high yield and purity using an aqueous process that is substantially lower in cost and GHG emissions by comparison to commodity plastics. Here, we lay foundations for tailoring the properties of PDK materials using highly functional and chiral BKDLs, which are best produced biosynthetically using hybrid PKSs. The architecture of the type I PKSs, whose modules and domains were recombined to define substitution and stereochemistry at specific carbons in the lactone ring, provides us with the ability to make diverse BKDLs. Using computational chemistry and experimental validation, we were able to explain why these substitutions alter the depolymerization temperature thresholds required for circularity. This discovery enables us to produce polymers that can be depolymerized under different conditions using the same biomanufacturing microbial chassis, something that would be nearly impossible to do at a scale using chemically synthesized BKDLs. The resulting BKDL-PDKs can be used to replace plastics used in electronics, building materials and automotive applications, as well as laminated materials and assemblies, and recover precursors in pristine quality for reuse. As shown in Supplementary Table 1, BKDL-PDKs differ from dimedone-PDK and TAL-PDK in both monomer architecture and predicted thermodynamic parameters, illustrating how biosynthetically accessible BKDL structures expand the design space of recyclable PDK materials.

It is important to emphasize why biosynthesis, rather than chemical synthesis, is the only viable manufacturing route for diverse chiral BKDLs at commodity scale. The chiral BKDLs required for tunable PDKs demand multistep stereoselective syntheses—Evans aldol reactions with chiral auxiliaries, pyrophoric reagents and carefully controlled reaction conditions—that are viable at milligram-to-gram scale for proof-of-concept studies but entirely impractical for commodity production. In contrast, engineered type I PKSs set both substitution pattern and stereochemistry in a single enzymatic step through module and domain recombination and the resulting BKDLs are secreted from the cell, simplifying downstream recovery. All PDKs characterized in this study were synthesized from chemically produced BKDL monomers, which are structurally identical to the biosynthetically produced BKDLs. The biosynthetic platform demonstrated here is designed to replace these chemical routes at commercial scale.

The tunability enabled by diverse BKDLs has practical implications beyond material properties. Because different BKDL-PDKs depolymerize at different temperatures spanning 0–60 °C, mixed-plastic streams containing multiple BKDL-PDK types can be recycled by sequential temperature steps—a staged recovery process in which each monomer is recovered cleanly at its specific depolymerization threshold. This temperature-gated recycling capability is unique among recyclable polymer families and enables a single microbial chassis to supply monomers for electronics (high T_g, solvent resistance), packaging (flexibility, lower T_g) and structural applications (mechanical durability)—all while maintaining full chemical recyclability.

Environmental impact categories beyond GHG emissions will ultimately be important and are worthy of further study. One of the most interesting potential impacts of scaling up biobased recyclable plastics could be changes in the release of microplastics; a recent review noted that LCAs can be updated to incorporate such metrics where relevant. Additionally, while we adopted a cradle-to-gate scope for this study (rather than cradle-to-cradle) to aid in comparison of BKDL-PDK to fossil-based PDKs produced from petroleum-based dimedone, a cradle-to-cradle scope that incorporates several possible recovery and recycling systems will be key to understanding the full system-wide impact, including microplastics and changes in total landfilled or incinerated waste. Nonetheless, the analysis presented here and elsewhere provides strong foundations for a more extensive scenario-based cradle-to-cradle exploration of the life-cycle impacts of BKDL-based PDKs. Our current system was modeled assuming a minimal medium for BKDL production (use of five-carbon and six-carbon sugars). Further commercialization would aid in exploration of an effective minimal medium and this is expected to happen as the technology becomes more established and the process is scaled up commercially.

Our TEA and life-cycle GHG inventory models demonstrate the potential economic advantages and emissions reduction of biobased BKDLs. The analysis shows that BKDL-based PDKs can be produced at a lower cost compared to previously published dimedone-based virgin PDKs[5]. The analysis also highlights where further optimization

is necessary; increases in the BKDL production rate and yield are the most important next steps for commercializing BKDL-PDKs because this enables greater production volumes in smaller bioreactors. Optimizing the production rate will also reduce electricity requirements for bioreactor aeration and agitation, thus driving down GHG emissions. While producing virgin PDK will remain more costly than petroleum-based plastics, its key advantage is the ease of recycling to virgin-quality monomers. Previously published results show that the price of circular PDK (1.5 US$ per kg) is competitive when compared to other commercial plastics such as HDPE, PU and PET (2.3, 4 and 1.2 US$ per kg, respectively)[5]. The substantial reduction in GHG emissions and cost achievable by using BKDL instead of dimedone for PDK synthesis opens new properties while simultaneously closing the cost and emissions gap between virgin and circular PDK.

Lastly, these new materials were developed through an intersectional research paradigm, where synthetic biology, computational, synthetic and polymer chemistry, TEAs and LCAs are merged for holistic understanding. In doing so, we identified a series of highly recyclable biopolymers with readily customizable properties enabled by a flexible, scalable microbial chassis to biosynthesize them from renewable feedstocks. We believe that this unique mode of collaboration could result in more sustainable bioeconomy solutions to some of the planet's biggest challenges.

Online content

Any methods, additional references, Nature Portfolio reporting summaries, source data, extended data, supplementary information, acknowledgements, peer review information; details of author contributions and competing interests; and statements of data and code availability are available at https://doi.org/10.1038/s41587-026-03229-7.

References

1. Geyer, R., Jambeck, J. R. & Law, K. L. Production, use, and fate of all plastics ever made. *Sci. Adv.* **3**, e1700782 (2017).
2. Jeswani, H. et al. Life cycle environmental impacts of chemical recycling via pyrolysis of mixed plastic waste in comparison with mechanical recycling and energy recovery. *Sci. Total Environ.* **769**, 144483 (2021).
3. Demeneix, B. A. How fossil fuel-derived pesticides and plastics harm health, biodiversity, and the climate. *Lancet Diabetes Endocrinol.* **8**, 462–464 (2020).
4. Christensen, P. R., Scheuermann, A. M., Loeffler, K. E. & Helms, B. A. Closed-loop recycling of plastics enabled by dynamic covalent diketoenamine bonds. *Nat. Chem.* **11**, 442–448 (2019).
5. Demarteau, J. et al. Circularity in mixed-plastic chemical recycling enabled by variable rates of polydiketoenamine hydrolysis. *Sci. Adv.* **8**, eabp8823 (2022).
6. He, C. et al. Conformational entropy as a means to control the behavior of poly(diketoenamine) vitrimers in and out of equilibrium. *Angew. Chem. Int. Ed. Engl.* **59**, 735–739 (2020).
7. Vora, N. et al. Leveling the cost and carbon footprint of circular polymers that are chemically recycled to monomer. *Sci. Adv.* **7**, eabf0187 (2021).
8. Demarteau, J. et al. Biorenewable and circular polydiketoenamine plastics. *Nat. Sustain.* **6**, 1426–1435 (2023).
9. Klaus, M. et al. Protein–protein interactions, not substrate recognition, dominate the turnover of chimeric assembly line polyketide synthases. *J. Biol. Chem.* **291**, 16404–16415 (2016).
10. Wu, N., Kudo, F., Cane, D. E. & Khosla, C. Analysis of the molecular recognition features of individual modules derived from the erythromycin polyketide synthase. *J. Am. Chem. Soc.* **122**, 4847–4852 (2000).
11. Eng, C. H. et al. ClusterCAD: a computational platform for type I modular polyketide synthase design. *Nucleic Acids Res.* **46**, D509–D515 (2018).
12. Tao, X. B. et al. ClusterCAD 2.0: an updated computational platform for chimeric type I polyketide synthase and nonribosomal peptide synthetase design. *Nucleic Acids Res.* **51**, D532–D538 (2023).
13. Englund, E. et al. Expanding extender substrate selection for unnatural polyketide biosynthesis by acyltransferase domain exchange within a modular polyketide synthase. *J. Am. Chem. Soc.* **145**, 8822–8832 (2023).
14. Floss, H. G. & Yu, T.-W. Rifamycin—mode of action, resistance, and biosynthesis. *Chem. Rev.* **105**, 621–632 (2005).
15. Hong, H., Demangel, C., Pidot, S. J., Leadlay, P. F. & Stinear, T. Mycolactones: immunosuppressive and cytotoxic polyketides produced by aquatic mycobacteria. *Nat. Prod. Rep.* **25**, 447–454 (2008).
16. Staunton, J. & Wilkinson, B. Biosynthesis of erythromycin and rapamycin. *Chem. Rev.* **97**, 2611–2630 (1997).
17. Chen, H., O'Connor, S., Cane, D. E. & Walsh, C. T. Epothilone biosynthesis: assembly of the methylthiazolylcarboxy starter unit on the EpoB subunit. *Chem. Biol.* **8**, 899–912 (2001).
18. Murli, S., Kennedy, J., Dayem, L. C., Carney, J. R. & Kealey, J. T. Metabolic engineering of *Escherichia coli* for improved 6-deoxyerythronolide B production. *J. Ind. Microbiol. Biotechnol.* **30**, 500–509 (2003).
19. Gläser, L. et al. A common approach for absolute quantification of short chain CoA thioesters in prokaryotic and eukaryotic microbes. *Microb. Cell Fact.* **19**, 160 (2020).
20. Miyazawa, T., Fitzgerald, B. J. & Keatinge-Clay, A. T. Preparative production of an enantiomeric pair by engineered polyketide synthases. *Chem. Commun.* **57**, 8762–8765 (2021).
21. Klass, S. H. et al. Engineering controllable alteration of malonyl-CoA levels to enhance polyketide production. *Nat. Chem. Biol.* **21**, 1214–1225 (2025).
22. Epstein, A. R., Demarteau, J., Helms, B. A. & Persson, K. A. Variable amine spacing determines depolymerization rate in polydiketoenamines. *J. Am. Chem. Soc.* **145**, 8082–8089 (2023).
23. Møller, K. H., Otkjær, R. V., Hyttinen, N., Kurtén, T. & Kjaergaard, H. G. Cost-effective implementation of multiconformer transition state theory for peroxy radical hydrogen shift reactions. *J. Phys. Chem. A* **120**, 10072–10087 (2016).
24. Bao, J. L. & Truhlar, D. G. Variational transition state theory: theoretical framework and recent developments. *Chem. Soc. Rev.* **46**, 7548–7596 (2017).
25. Cao, M. et al. Metabolic engineering of oleaginous yeast *Rhodotorula toruloides* for overproduction of triacetic acid lactone. *Biotechnol. Bioeng.* **119**, 2529–2540 (2022).

[1]QB3 Institute, University of California, Berkeley, Berkeley, CA, USA. [2]Department of Chemical and Biomolecular Engineering, University of California, Berkeley, Berkeley, CA, USA. [3]Joint BioEnergy Institute, Emeryville, CA, USA. [4]The Molecular Foundry, Lawrence Berkeley National Laboratory, Berkeley, CA, USA. [5]Department of Materials Science and Engineering, University of California, Berkeley, Berkeley, CA, USA. [6]Biological Systems and Engineering Division, Lawrence Berkeley National Laboratory, Berkeley, CA, USA. [7]Department of Chemistry, University of California, Berkeley, Berkeley, CA, USA. [8]Department of Molecular and Cell Biology, University of California, Berkeley, Berkeley, CA, USA. [9]Energy Analysis Division, Lawrence Berkeley National Laboratory, Berkeley, CA, USA. [10]Novo Nordisk Foundation Center for Biosustainability, Technical University of Denmark, Lyngby, Denmark. [11]Biotechnology Research Institute for the Green Transition (BRIGHT), Department of Biotechnology and Biomedicine, Technical University of Denmark, Lyngby, Denmark. [12]Department of Plant and Microbial Biology, University of California, Berkeley, Berkeley, CA, USA. [13]Materials Sciences Division, Lawrence Berkeley National Laboratory, Berkeley, CA, USA. [14]Energy & Biosciences Institute, University of California, Berkeley, Berkeley, CA, USA. [15]Department of Bioengineering, University of California, Berkeley, Berkeley, CA, USA. [16]Present address: FutureBio, Inc., Berkeley, CA, USA. [17]Present address: The Dow Chemical Company, Collegeville, PA, USA. [18]Present address: Department of Chemistry, Durham University, Durham, UK. [19]Present address: School of Food and Biological Engineering, Jiangsu University, Jiangsu, China. [20]Present address: State Key Laboratory of Biology of Plant Diseases and Insect Pests, Institute of Plant Protection, Chinese Academy of Agricultural Sciences, Beijing, China. [21]Present address: Amazon.com, Inc., Seattle, WA, USA. [22]Present address: Department of Chemical and Biomolecular Engineering, University of Illinois Urbana-Champaign, Champaign, IL, USA. [23]Present address: BRIGHT, Technical University of Denmark, Lyngby, Denmark. ✉e-mail: keasling@berkeley.edu

Methods

Construction of PKS genes

The genes encoding the candidate modules in this study were either cloned from genomic DNA or synthesized and assembled in *Saccharomyces cerevisiae* (Supplementary Table 10). The yeast assembly protocol[26] was slightly modified to use in this study. While relatively small by natural PKS standards, these hybrid PKSs are large, multidomain enzymes; thus, we used two strategies to engineer them. The first strategy encoded the loading and first extension modules in one open reading frame (ORF) and the second extension module and TE in the second ORF, with DNA encoding intermodular linkers placed at the 3′ end of the gene encoding the first extension module and at the 5′ end of the gene encoding the second extension module. In the second strategy, we placed the loading module, extension modules 1 and 2 and TE within a single ORF (Supplementary Fig. 17). More than 40 recombined PKSs were constructed to study BKDL production in this study (Supplementary Table 3).

Integration of *pks* genes into *Streptomyces*

Both biparental conjugation and triparental conjugation were used in this study. Biparental conjugation was used as described in Practical *Streptomyces* Genetics[27] with slight modifications. For the biparental conjugation, *E. coli* ET12567 carrying pUZ8002 was transformed with a desired plasmid through selection on Luria–Bertani (LB) agar containing apramycin (50 mg L^{-1}) (Supplementary Table 11). A single colony was inoculated into 5 ml of LB containing kanamycin (25 mg L^{-1}), chloramphenicol (15 mg L^{-1}) and apramycin (25 mg L^{-1}) and grown at 37 °C. Overnight culture was used to seed 10 ml of LB containing the same antibiotics (inoculum size was 5% by volume), which was grown at 37 °C to an optical density at 600 nm (OD_{600}) of 0.4–0.6, which usually takes 4–6 h. The *E. coli* cells were pelleted by centrifugation at 3,000*g* for 5 min, washed twice with 10 ml of LB and resuspended in 1 ml of LB. Fresh *Streptomyces* spores were collected from a mannitol soy (MS) agar plate with 5 ml of 2× YT and incubated at 50 °C for 10 min. MS agar was prepared by adding 20 g of agar, 20 g of mannitol and 20 g of soybean flour to 1 L of tap water and autoclaved. After autoclaving and cooling, magnesium chloride was added at 10 mM. The spores (500 µl) and the *E. coli* cells (500 µl) were mixed and briefly centrifuged at 3,000*g* for 2 min. Most of the supernatant was poured off and spread on MS agar and incubated at 30 °C for 16–20 h. After the addition of 1 ml of water containing nalidixic acid (0.5 g L^{-1}) and apramycin (1.25 g L^{-1}), the plate was further incubated for 3–5 days to permit sporulation.

For the triparental conjugation, *E. coli* DH5α carrying PKS plasmid and *E. coli* ET12567 carrying helper plasmid pUB307 were inoculated into 10 ml of LB (25 µg ml^{-1} chloramphenicol and 50 µg ml^{-1} kanamycin) and grown overnight at 37 °C. Then, 100 µl of overnight culture was inoculated into 10 ml of fresh LB plus antibiotics as above and grown for ~4 h at 37 °C to an OD_{600} of 0.4–0.6. The cells were washed twice with 10 ml of LB to remove antibiotics that might inhibit *Streptomyces* growth. *E. coli* ET12567 with pUB307 was resuspended in 0.5–1 ml of LB and *E. coli* DH5α with PKS plasmid was resuspended in 0.2–0.4 ml of LB. While washing the *E. coli* cells, 10–20 µl of *Streptomyces* spores were added to 200 µl of 2× YT broth, heat-shocked at 50 °C for 10 min and then allowed to cool. Next, 0.1 ml of each *E. coli* cell suspension and 0.2 ml of heat-shocked spores were mixed. Then, 50 µl and 350 µl of each mixture were plated onto two MS agar plates containing 10 mM $MgCl_2$ (without antibiotics) and incubated at 30 °C for 16–20 h. The plates were overlaid with 1.0 ml of water containing 0.5 mg of nalidixic acid (20 µl of 25 mg ml^{-1} stock; to selectively kill *E. coli*) and 2–4 mg of kanamycin (40 µl of 50 mg ml^{-1} stock). Gentle shaking was performed to lightly distribute the antibiotic solution evenly and the plates were incubated at 30 °C.

Protein purification

Cell stocks were inoculated into 10 ml of LB broth containing 50 µg ml^{-1} kanamycin, incubated at 37 °C overnight at 225 rpm. This seed culture was used to inoculate 1 L of LB broth containing 50 µg ml^{-1} kanamycin and then incubated at 37 °C for 2 to 3 h at 225 rpm. When the OD_{600} reached 0.6, the culture was cooled on ice for 15–20 min. Next, 0.2 mM IPTG was added to induce protein expression and the culture was incubated at 18 °C to allow protein expression. Cells were harvested by centrifugation at 7,000*g* at 4 °C. Harvested cells were transferred to a 50-ml Falcon tube kept at −80 °C until needed. Pellets from 1 L of cell culture were thawed at room temperature and resuspended in 10 ml of cell lysis buffer (50 mM NaH_2PO_4:NaOH pH 7.8, 300 mM NaCl and 10 mM PMSF). The cells were lysed by sonication for 15 min (500 W, 30% amplitude, pulse: 5 s on and 10 s off). Cell debris and other insoluble material were removed by centrifugation for 45 min at 13,000*g* at 4 °C. The soluble fraction was filtered using a 0.22-µm filter, mixed with 1 ml of Ni-NTA resin (Thermo Scientific) and incubated at 4 °C for 1 h under constant mixing. The resulting resin was washed with wash buffer (50 mM sodium phosphate pH 7.8, 0.3 M NaCl and 20 mM imidazole) and the target protein was eluted using the elution buffer (50 mM sodium phosphate pH 7.8, 0.3 M NaCl and 200 mM imidazole).

In vitro BKDL production with purified proteins

The 200-µl reaction mixture contained 5 µM purified protein of module 2, 1 mM (*S*)-*N*-acetylcysteine substrate (Supplementary Fig. 2a), 2.5 mM DTT, 1 mM EDTA, 0.2 mM malonyl-CoA, 100 mM phosphate adjusted to pH 7.4 and 10% glycerol. The reaction mixture was incubated at room temperature for 24 h. The samples were quenched by mixing with 200 µl of acetonitrile with 0.05 mM internal standard and analyzed by liquid chromatography–mass spectrometry (LC–MS) (Supplementary Table 12).

In vitro BKDL production with dialyzed cell lysate

The glycerol stock of the *E. coli* BAP1 with *pks* genes was inoculated in 5 ml of LB overnight at 30 °C, followed by scaling up the cell cultures in 200 ml of LB at 30 °C. The PKS expression was induced at OD_{600} = 0.6 with 0.2 mM IPTG at 18 °C for 20 h. Cells were harvested and lysed in 20 ml of lysis buffer (50 mM sodium phosphate pH 7.4, 0.3 M NaCl and 5% glycerol) with sonication. The soluble PKS expression level was evaluated by SDS–PAGE analysis. The 20-ml cell lysate was dialyzed with the dialysis tubing (SnakeSkin, Thermo) to 2 L of 100 mM sodium phosphate buffer pH 7.4, 100 mM NaCl, 5% glycerol and 2.5 mM DTT at 4 °C for 16 h. The dialyzed cell lysate was filtered with a 0.2-µm filter and concentrated tenfold. The 200-µl reaction mixture contained cell lysate with a comparable expression level of loading module, module 1 and module 2, as well as 2.5 mM DTT, 1 mM EDTA, 0.2 mM starter CoA ester (acetyl-CoA or propionyl-CoA), 0.2 mM first extender CoA ester (malonyl-CoA or methylmalonyl-CoA), 0.2 mM second extender CoA ester (malonyl-CoA) and 4 mM NADPH. The reaction mixture was incubated at room temperature for 48 h. The samples were quenched by mixing with 200 µl of acetonitrile and 0.05 mM internal standard and analyzed by LC–MS (Supplementary Table 12).

In vivo BKDL production

For high-throughput cultivation, engineered *S. albus* spores (5 µl) were grown in 0.5 ml of tryptic soy broth (TSB) containing nalidixic acid (25 mg L^{-1}) for 2 days at 30 °C in a 96-well plate to reach $OD_{600} \geq 1.0$ as the seed culture. This seed culture was adjusted to the cell density at OD_{600} = 1.0 and spun down to collect the cell pellets. After discarding the supernatant, 0.5 ml of R5 medium containing nalidixic acid (25 mg L^{-1}) was added to each well. One 4.5-mm sterile glass bead was added to each well. The plate was incubated at 30 °C at 200 rpm with 50% humidity for 5–10 days (Supplementary Fig. 5g–h).

For production of BKDLs by *Streptomyces* in flasks, engineered *S. albus* spores (50 µl) were grown in 4 ml of TSB containing nalidixic acid (25 mg L^{-1}) for 2 days at 30 °C to reach $OD_{600} \geq 1.5$ as the seed culture. This seed culture was adjusted to the cell density at OD_{600} = 1.5 and transferred to a 250-ml baffled flask containing 30 ml of R5 medium and

nalidixic acid (25 mg L^{-1}), fitted with a silicone sponge cap. The culture was grown for 7–11 days at 30 °C at 200 rpm with 50% humidity. Then, 10 ml of the resulting cell cultures were harvested on the day 7 and day 11. The production of BKDL was greatly improved by the addition of 10–20 0.45-mm sterile glass beads and 20 g L^{-1} Talc to break cell clumps[28] (Supplementary Fig. 10a).

For the production of BKDLs by *E. coli*, cells were first grown in LB at 30 °C overnight as seed cultures. Then, seed cultures (1% by volume) were inoculated in 2.5 ml of EZ-rich medium (Teknova) with some modifications: supplementations of 10 g L^{-1} tryptone, 5 g L^{-1} yeast extract, 5 mM calcium pantothenate and 20 g L^{-1} glycerol and replacement of 1.32 mM K_2HPO_4 with 2.8 mM Na_2HPO_4 (ref. 29), contained in 24-well plates. Cells were first incubated at 30 °C for 3–4 h and supplemented with 20 mM propionate and 100 µM IPTG inducer. Induced cells were then grown for 72 h at 18 °C until sample collection. During the growth, plates were sealed with breathable films and shaken at 200 rpm, before collecting 100 µl of cell cultures for analysis.

Bioreactor cultivation

The starter culture was prepared by inoculating a single colony of *E. coli* strain sSC26_2, the K207-3::*matB matC*[21] strain carrying plasmid to express Pik127 swapped with PikAT2 in module 2, in 5 ml of LB broth with 100 µg ml^{-1} carbenicillin and 50 µg ml^{-1} kanamycin at 30 °C overnight. Then, 1 ml of the starter culture was inoculated into 50 ml of LB-EZ-rich medium with the same antibiotics for adaptation at 30 °C for 16 h. Next, 15–17 ml of this seed culture was injected into the Sartorius bioreactors with the LB-EZ-rich medium to reach an OD_{600} of 0.1. The cells were grown at 30 °C, with 1.5 standard L per min of ambient air and internal rotor agitation in cascade mode, maintaining 20% dissolved oxygen. The pH was controlled at 7.0 using 10% (v/v) H_2SO_4 and 14% (v/v) NH_4OH. Protein expression was induced with 0.1 mM IPTG and 20 mM propionate and 20 mM malonate were added after 4 h; the temperature was then adjusted to 18 °C. Glycerol or glucose manual feeding started when the initial amount of glycerol or glucose concentration dropped below 5 g L^{-1} with a feed solution containing 600 g L^{-1} glycerol or glucose and 50 mg L^{-1} carbenicillin. Next, 5-ml samples were taken in regular intervals and centrifuged at 5,000*g* for 5 min to obtain the supernatant. For analysis, the supernatant was filtered (0.2 µm) and stored at −20 °C, while the cell pellet was stored at −80 °C.

LC–MS analysis

LC–MS was performed using an Agilent LC-MSD and a 6520 quadrupole time-of-flight MS system (Agilent Technologies). Both in vitro and in vivo, 50–100-µl samples were mixed with an equal volume of 100% acetonitrile containing internal standard, TAL, followed by filtration with a 96-well plate (3-kDa molecular weight cutoff; Pall Corporation). A Kinetex XB-C18 2.6-µm column (3 mm × 100 mm; Phenomenex) was used for LC separation of the molecules. A 3-µl sample was injected into the LC–MS system for analysis. Mobile phase A was water with 0.1% formic acid and mobile phase B was methanol with 0.1% formic acid. The detailed LC conditions are described in the Supplementary Methods. The MS was run in either negative or positive ion mode. For quantification of the MS peak area, all peak areas were calibrated by the internal standard signal.

TEA and GHG LCA of BKDL production

The first step to conducting scenario analysis is establishing stoichiometrically maximum achievable yields. We calculated the stoichiometric maximum theoretical yield of BKDL from glucose to be 0.547 g g^{-1} glucose. For all scenarios considered in this study, we assumed the xylose-to-BKDL conversion to be 90% of that of the glucose-to-BKDL conversion. BKDL bioproduction process models used in this study were developed in a commercial process modeling software package (SuperPro Designer-V12; Intelligen). The biorefinery operates 330 days per year and 24 h per day (equivalent to 90% uptime). Capital cost accounts for equipment purchase cost, installation costs, warehouse, site development, permits, land and other field expenses and project contingency costs. Annual operating cost accounts for materials, utilities, repair and maintenance, labor, and waste disposal costs. The assumptions for the model are consistent with Humbird et al.[30] unless otherwise specified. The bulk prices for material costs were obtained from peer-reviewed literature, market price reports, and Alibaba. Equipment purchase prices were derived using built-in cost estimating functions available in SuperPro. The process parameters and assumptions for the different scenarios are shown in Supplementary Tables 13–18. Additionally, description and major assumptions for each of the major biomass-to-BKDL production systems are presented in the Supplementary Information and are consistent with the assumptions by Demarteau et al.[8].

All results are reported in terms of BKDL MSP, which determines the selling price needed to reach a net present value of zero given a 10% internal rate of return. 'This work' represents a scenario where experimental yield with glucose is used, extrapolated to xylose assuming commercial production would use a microbial host capable of using five-carbon and six-carbon sugars. The intermediate scenario reflects a future in which 50% of theoretical maximum yield is achievable. All other aspects of the scenario (such as temperature, retention time and host used at the bioconversion unit) reflect those in the experimental work of this study. Specifically, the intermediate scenario represents 50% of the theoretical maximum BKDL yield from glucose, extrapolated to xylose (0.27 g BKDL g^{-1} glucose and 0.24 g BKDL g^{-1} xylose). The optimized scenario represents a mature facility in which the BKDL yield reaches approximately 90% of the stoichiometric theoretical maximum (0.49 g BKDL g^{-1} glucose and 0.44 g BKDL g^{-1} xylose) and all other process parameters have been optimized to reach a practical minimum production cost, including a reduction in residence time from 27 to 24 h. The mass/energy balances and the major costs and revenues associated with the bioproduction of BKDL are presented in Supplementary Tables 14–16. Modeling inputs and assumptions for bioproduction of BKDL are summarized in Supplementary Table 17.

The system boundary for the GHG assessment of bioproduction of BKDL is cradle-to-gate. This system boundary was selected because the goal of this study was to enable comparisons between fossil-derived dimedone and BKDLs as an input to BKDL-PDK production. The functional unit for the analysis is defined as 1 kg of BKDL produced, which can be compared to 1 kg of dimedone. The life-cycle GHG inventory was completed using a hybrid process-based/physical unit-based input/output approach and the life-cycle inventory data and characterization factors for input materials and commodity polymers were obtained from peer-reviewed studies[7,31,32], LCA databases including Ecoinvent[33], US Life Cycle Inventory (https://www.lcacommons.gov), GREET (https://greet.anl.gov/) and WARM (https://www.epa.gov/waste-reduction-model). The input parameters for the life-cycle GHG inventory model of the three scenarios used in this study, the emission factors associated with the unit processes and the input/output matrix relationships are tabulated in Supplementary Tables 18–20, respectively, and more details regarding the input/output life-cycle inventory model can be found in the Supplementary Information. Our analysis treats biogenic ('contemporary') carbon as part of a closed cycle, in which biogenic CO_2 emitted during bioconversion is taken up when feedstock crops are regrown because our system relies on biomass from an annual crop (corn stover). Other approaches would be needed for a system relying on slower-growing feedstocks, such as forest biomass. To account for the biogenic carbon in the BKDL (and, ultimately, in BKDL-PDK), we conservatively assume that there is no net accumulation or sink of biogenic carbon in the long term. Realistically, there will be a small stock of biogenic carbon accumulated in PDK plastics that are continually recycled (and not oxidized) but we expect the long-term impact of this stock on net emissions to be small. In this study, we assume the GHG emissions footprint for dimedone to be

8 kg CO_2e per kg of dimedone, according to dimedone emission values reported in previous work[4].

Reporting summary

Further information on research design is available in the Nature Portfolio Reporting Summary linked to this article.

Data availability

The data in this study are available within the article and its Supplementary Information. The DNA sequences of plasmids and strains used in this study were deposited to the Joint BioEnergy Institute public registry (http://public-registry.jbei.org). Accession codes are provided in Supplementary Table 2. The MS proteomics data were deposited to the PRIDE repository under accession code PXD042863. Data are also available from the authors upon request. Source data are provided with this paper.

Code availability

No custom code central to the conclusions of this study was generated. Software, scripts and computational tools used in this study are described in Methods, Supplementary Methods and Nature Portfolio Reporting Summary.

References

26. Ip, K., Yadin, R. & George, K. W. High-throughput DNA assembly using yeast homologous recombination. *Methods Mol. Biol.* **2205**, 79–89 (2020).
27. Kieser, T., Bibb, M. J., Buttner, M. J., Chater, K. F. & Hopwood, D. A. *Practical Streptomyces Genetics* (John Innes Foundation, 2000).
28. Kuhl, M. et al. Microparticles globally reprogram *Streptomyces albus* toward accelerated morphogenesis, streamlined carbon core metabolism, and enhanced production of the antituberculosis polyketide pamamycin. *Biotechnol. Bioeng.* **117**, 3858–3875 (2020).
29. Clomburg, J. M., Vick, J. E., Blankschien, M. D., Rodríguez-Moyá, M. & Gonzalez, R. A synthetic biology approach to engineer a functional reversal of the β-oxidation cycle. *ACS Synth. Biol.* **1**, 541–554 (2012).
30. Humbird, D. et al. *Process Design and Economics for Biochemical Conversion of Lignocellulosic Biomass to Ethanol: Dilute-Acid Pretreatment and Enzymatic Hydrolysis of Corn Stover* Report No. NREL/TP-5100-47764 (National Renewable Energy Laboratory, 2011).
31. Kyulavska, M., Toncheva-Moncheva, N. & Rydz, J. in *Handbook of Ecomaterials* (eds Martínez, L. M. T. et al.) 1–34 (Springer, 2017).
32. Amelio, A., Genduso, G., Vreysen, S., Luis, P. & Van der Bruggen, B. Guidelines based on life cycle assessment for solvent selection during the process design and evaluation of treatment alternatives. *Green Chem.* **16**, 3045–3063 (2014).
33. Wernet, G. et al. The ecoinvent database version 3 (part I): overview and methodology. *Int. J. Life Cycle Assess.* **21**, 1218–1230 (2016).

Acknowledgements

This work was supported by the US Department of Energy (DOE) Bioenergy Technologies Office award number 1916-1597, the Joint BioEnergy Institute (https://www.jbei.org), which is supported by the DOE, Office of Science, Office of Biological and Environmental Research under contract DE-AC02-05CH11231, the Philomathia Foundation and the Nancy P. and Richard K. Robins Family Foundation. Portions of this work, including PDK synthesis, characterization and deconstruction, were carried out as a User Project at the Molecular Foundry, which is supported by the Office of Science, Office of Basic Energy Sciences of the US DOE under contract no. DE-AC02-05CH11231. A.R.E. was supported by the National Science Foundation Graduate Research Fellowship under grant no. DGE 1752814. Data for this study were produced using the Savio computational cluster resource provided by the Berkeley Research Computing program at the University of California, Berkeley (supported by the University of California, Berkeley Chancellor, Vice Chancellor for Research and Chief Information Officer). We thank C. Fortman for his help with the project management. We thank B. Moore for providing the strain of *E. coli* ET12567(pUB307) applied in *Streptomyces* triparental conjugation. We thank A. Keatinge-Clay for providing the strain of *E. coli* K207-3 (Pik127 and Pik167). We also thank C. Khosla for providing the plasmid of pBL12-LDD(4) for in vitro production. The United States Government retains and the publisher, by accepting the article for publication, acknowledges that the United States Government retains, a nonexclusive, paid-up, irrevocable, worldwide license to publish or reproduce the published form of this manuscript, or allow others to do so, for United States Government purposes. Any subjective views or opinions that might be expressed in this paper do not necessarily represent the views of the US Department of Energy or the United States Government.

Author contributions

All authors contributed to the conceptualization of the project. J.D.K., Z.W., S.C., A.R.E., J.D. and B.B. wrote the original paper with input from all the other authors. J.D.K., R.W.H., B.A.H., C.D.S. and K.A.P. guided the project. Z.W., S.C., R.W.H., W.H., L.K., M.S., A.A.N., M.Z., B.G., Y.G. and Y.L. conducted the experiments of cloning and BKDL biosynthesis. P.C.-M. and K.Y. conducted the genome mining of PKS candidates. A.R.E. and R.G. contributed to the methodology of PDK computation modeling. H.W. conducted the experiments of precursor synthesis for in vitro BKDL formation. H.W. and J.D. conducted the experiments of PDK synthesis and recycling. B.B., N.V., S.L.N. and N.R.B. contributed to the TEA and life-cycle GHG inventory modeling. R.K. and E.E.K.B. performed the LC–MS. Y.C. and C.J.P. performed the proteomics analysis. All authors contributed to writing the final draft and editing. J.D.K., B.A.H., C.D.S. and K.A.P. acquired funding.

Competing interests

J.D.K. has financial interest in Demetrix, Maple Bio, Lygos, Napigen, Berkeley Yeast, Zero Acre Farms, Ansa Biotechnologies, Apertor Pharmaceuticals and ResVita Bio. B.A.H., J.D.K. and C.D.S. have financial interest in Cyklos Materials. Z.W. and S.C. have financial interest in FutureBio. The other authors declare no competing interests.

Additional information

Supplementary information The online version contains supplementary material available at https://doi.org/10.1038/s41587-026-03229-7.

Correspondence and requests for materials should be addressed to Jay D. Keasling.

Peer review information *Nature Biotechnology* thanks the anonymous reviewers for their contribution to the peer review of this work.

nature portfolio

Corresponding author(s): Jay D. Keasling

Last updated by author(s): May 28, 2026

Reporting Summary

Nature Portfolio wishes to improve the reproducibility of the work that we publish. This form provides structure for consistency and transparency in reporting. For further information on Nature Portfolio policies, see our Editorial Policies and the Editorial Policy Checklist.

Statistics

For all statistical analyses, confirm that the following items are present in the figure legend, table legend, main text, or Methods section.

n/a	Confirmed	
☐	☒	The exact sample size (*n*) for each experimental group/condition, given as a discrete number and unit of measurement
☐	☒	A statement on whether measurements were taken from distinct samples or whether the same sample was measured repeatedly
☒	☐	The statistical test(s) used AND whether they are one- or two-sided *Only common tests should be described solely by name; describe more complex techniques in the Methods section.*
☒	☐	A description of all covariates tested
☒	☐	A description of any assumptions or corrections, such as tests of normality and adjustment for multiple comparisons
☒	☐	A full description of the statistical parameters including central tendency (e.g. means) or other basic estimates (e.g. regression coefficient) AND variation (e.g. standard deviation) or associated estimates of uncertainty (e.g. confidence intervals)
☒	☐	For null hypothesis testing, the test statistic (e.g. *F*, *t*, *r*) with confidence intervals, effect sizes, degrees of freedom and *P* value noted *Give P values as exact values whenever suitable.*
☒	☐	For Bayesian analysis, information on the choice of priors and Markov chain Monte Carlo settings
☒	☐	For hierarchical and complex designs, identification of the appropriate level for tests and full reporting of outcomes
☒	☐	Estimates of effect sizes (e.g. Cohen's *d*, Pearson's *r*), indicating how they were calculated

Our web collection on statistics for biologists contains articles on many of the points above.

Software and code

Policy information about availability of computer code

Data collection	All quantum chemistry calculations were performed using CREST and Gaussian16. All pre- and post-processing of calculations was done using Pymatgen. We measured the cell growth on SpectraMax M2. We quantified BKDL on Agilent LC-MSD and a 6520 Quadrupole Time-of-Flight Mass Spectrometer system (Agilent Technologies, Santa Clara, USA). and a reverse phase column (Kinetex XB-C18, 2.6 µm, 3 mm x 100 mm column (Phenomenex, USA)). 1H, 13C and HSQC solution state NMR spectroscopy was carried out using a Bruker Avance II at 500 and 125 MHz. DSC data were acquired using a TA Instruments Q200. We obtained life-cycle inventory data and characterization factors for input materials and commodity polymers from peer-reviewed literature, and LCA databases including Ecoinvent, US Life Cycle Inventory (USLCI), GREET, and WARM models and experimental data in this study.
Data analysis	We conducted the process modeling in SuperPro Designer software (SuperPro Designer. Intelligen: Scotch Plains, NJ.). We conducted the LC-MS data analysis in Agilent OpenLab and MassHunter software. We conducted 1H, 13C and HSQC NMR analysis using Bruker TopSpin 4.1.1 software. DSC data were analyzed using a TA Instruments TRIOS software.

For manuscripts utilizing custom algorithms or software that are central to the research but not yet described in published literature, software must be made available to editors and reviewers. We strongly encourage code deposition in a community repository (e.g. GitHub). See the Nature Portfolio guidelines for submitting code & software for further information.

Data

Policy information about availability of data

All manuscripts must include a data availability statement. This statement should provide the following information, where applicable:

- Accession codes, unique identifiers, or web links for publicly available datasets
- A description of any restrictions on data availability
- For clinical datasets or third party data, please ensure that the statement adheres to our policy

The authors declare that the data in this study are available within the paper and its Supplementary Information. The DNA sequences of plasmids and strains used in this study are deposited in the JBEI Public Registry (http://public-registry.jbei.org). Accession codes are provided in Supplementary Tables 2. The MS proteomics data are deposited at the PRIDE repository with accession code PXD042863. Source data are also provided with this paper. These data are also available from the authors upon request.

Research involving human participants, their data, or biological material

Policy information about studies with human participants or human data. See also policy information about sex, gender (identity/presentation), and sexual orientation and race, ethnicity and racism.

Reporting on sex and gender	N/A
Reporting on race, ethnicity, or other socially relevant groupings	N/A
Population characteristics	N/A
Recruitment	N/A
Ethics oversight	N/A

Note that full information on the approval of the study protocol must also be provided in the manuscript.

Field-specific reporting

Please select the one below that is the best fit for your research. If you are not sure, read the appropriate sections before making your selection.

☒ Life sciences ☐ Behavioural & social sciences ☐ Ecological, evolutionary & environmental sciences

For a reference copy of the document with all sections, see nature.com/documents/nr-reporting-summary-flat.pdf

Life sciences study design

All studies must disclose on these points even when the disclosure is negative.

Sample size	Sample sizes were generally three or more biological replicates unless otherwise indicated.
Data exclusions	No data was excluded in the processing of data analysis.
Replication	Production experiments were performed with three or more biological replicates. Product confirmation and screening experiments were performed with two or more biological replicates. The proteomics were performed with two or more replicates.
Randomization	Single colonies were randomly selected from agar plates for strain characterization experiments.
Blinding	Blinding was not relevant to this study.

Reporting for specific materials, systems and methods

We require information from authors about some types of materials, experimental systems and methods used in many studies. Here, indicate whether each material, system or method listed is relevant to your study. If you are not sure if a list item applies to your research, read the appropriate section before selecting a response.

Materials & experimental systems

n/a	Involved in the study
☒	☐ Antibodies
☒	☐ Eukaryotic cell lines
☒	☐ Palaeontology and archaeology
☒	☐ Animals and other organisms
☒	☐ Clinical data
☒	☐ Dual use research of concern
☒	☐ Plants

Methods

n/a	Involved in the study
☒	☐ ChIP-seq
☒	☐ Flow cytometry
☒	☐ MRI-based neuroimaging